

Spatial Resolution in Photoacoustic Tomography: Effects of Detector Size and Detector Bandwidth

Markus Haltmeier and Gerhard Zangerl

Computational Science Center, University of Vienna,
Nordbergstraße 15, A-1090 Wien.

E-mail: `Markus.Haltmeier@univie.ac.at`

May 3, 2010

High spatial resolution is one of the major aims in tomographic imaging. Two main factors limiting the resolution of photo- and thermoacoustic tomography are the detector size and the finite bandwidth of the ultrasound detection system. In this paper we present a quantitative analysis of those effects for “approximate point detectors” and for “approximate line detectors”.

Keywords. Photoacoustic tomography; thermoacoustic; tomography; image reconstruction; wave equation; resolution; bandwidth.

AMS classifications. 44A12, 65R32, 35L05, 92C55.

1 Introduction and main results

Photoacoustic tomography (PAT) is new imaging modality for visualizing the optical absorption coefficient of a probe. It has proven great promise for a variety of biomedical applications, such as imaging of animals, early cancer diagnostics, and imaging of vasculature (see [9, 21, 27, 30, 38, 39, 40, 43]). PAT is based on the excitation of acoustic pressure waves by illuminating a probe with short light pulses. The acoustic pressure is recorded outside of the object and used to reconstruct an image of the probe. We refer the reader to [36, Section 1.5] for a detailed mathematical description.

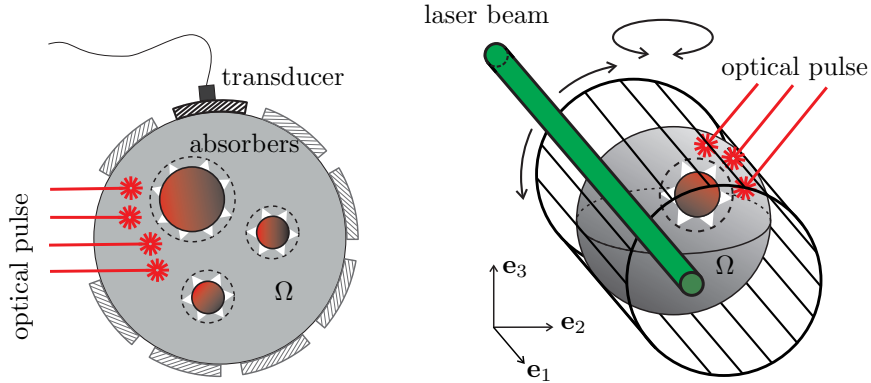


Figure 1: Photoacoustic tomography with piezoelectric transducer as an “approximate point detector” (left) and a laser beam as “approximate line detector” (right).

If we assume that the probe is acoustically homogeneous, the induced acoustic pressure $p : \mathbb{R}^3 \times (0, \infty) \rightarrow \mathbb{R}$ satisfies

$$(\partial_t^2 - \Delta) p(\mathbf{x}, t) = 0, \quad (\mathbf{x}, t) \in \mathbb{R}^3 \times (0, \infty), \quad (1a)$$

$$p(\mathbf{x}, 0) = f(\mathbf{x}), \quad \partial_t p(\mathbf{x}, 0) = 0, \quad \mathbf{x} \in \mathbb{R}^3, \quad (1b)$$

where Δ denotes the Laplacian with respect to the spatial variable \mathbf{x} and ∂_t is the derivative with respect to the temporal variable t . The goal of PAT is to reconstruct the initial pressure f (representing the probe) from measurements of $p(\mathbf{x}, t)$ taken outside of Ω . We assume throughout that initial pressure f is an element of the space $C_c^\infty(\Omega)$ of all smooth functions with compact support in Ω .

We denote by $\mathcal{W}^{3D} : C_c^\infty(\mathbb{R}^3) \rightarrow C^\infty(\mathbb{R}^3 \times (0, \infty))$ the operator that maps the compactly supported $f \in C_c^\infty(\mathbb{R}^3)$ to the solution of (1a), (1b).

1.1 Approximate point detectors

The classical approach in PAT is to assume that point-wise measured data

$$(\mathbf{P} f)(\mathbf{x}, t) := g(\mathbf{x}, t) := (\mathcal{W}^{3D} f)(\mathbf{x}, t), \quad \text{with } (\mathbf{x}, t) \in \partial\Omega \times (0, \infty),$$

are given (see [22, 23, 43]). The operator $\mathbf{P} : C_c^\infty(\Omega) \rightarrow C^\infty(\partial\Omega \times (0, \infty))$ that maps the initial data of the wave equation to the data measured by an ideal point detector can be inverted uniquely (see [2, 3]) and stably (see [26, 31, 45]). Analytic expressions for its inverse

$$\mathbf{P}^{-1} : \text{ran}(\mathbf{P}) \subset C^\infty(\partial\Omega \times (0, \infty)) \rightarrow C_c^\infty(\Omega)$$

via eigenfunction expansions are derived in [1, 25]. (Here $\text{ran}(\mathbf{P}) := \{\mathbf{P} f : f \in C_c^\infty(\Omega)\}$ denotes the range of \mathbf{P} .) Efficient reconstruction methods for arbitrary Ω are based on time reversal (see [7, 8, 11, 18, 19, 37]). In the case that Ω is a ball, filtered back-projection type inversion formulas are derived in [11, 24, 29, 42].

In practical applications, the detection system has a finite bandwidth. Moreover, standard ultrasound transducers, which integrate the pressure over its surface, are used to approximate point data (see [41]). We assume for simplicity that the transducer surface is part of the measurement surface. Then, the data measured by approximate point detectors are given by (see [41])

$$(\mathbf{P}_{\phi,w} f)(\mathbf{x}, t) = \left[\phi *_t \int_{\partial\Omega} w(\mathbf{x}, \mathbf{x}') (\mathcal{W}^{3D} f)(\mathbf{x}', \cdot) dS(\mathbf{x}') \right] (t),$$

for $(\mathbf{x}, t) \in \partial\Omega \times (0, \infty)$. (2)

Here $w(\mathbf{x}, \cdot)$ represents the sensitivity of the detector located at position $\mathbf{x} \in \partial\Omega$, $\phi(t)$ denotes the impulse response function of the ultrasound detection system, and $*_t$ is the convolution with respect to the temporal variable t .

Inexact knowledge of w and ϕ , as well as the ill-posedness of deblurring problems make it impossible to stably reconstruct the function f from the data in (2). It is therefore common to apply the exact inverse of \mathbf{P} to the data $\mathbf{P}_{\phi,w} f$. This results in a blurred reconstruction, where the blurring depends on the detector size and the detector bandwidth.

For the following result we assume that $\Omega = B_R$ is a ball of radius R and that the detector surface is rotationally symmetric (see Figure 1), that is, we have $w(\mathbf{x}, \mathbf{x}') = w_{\text{point}}(|\mathbf{x} - \mathbf{x}'|)$ for some univariate function w_{point} .

Theorem 1.1. *Let $f \in C_c^\infty(B_R)$, and let $\phi, w_{\text{point}} : \mathbb{R} \rightarrow \mathbb{R}$ be even functions such that $\mathbf{x} \in \mathbb{R}^3 \mapsto \phi'(|\mathbf{x}|)/|\mathbf{x}|$ and $\mathbf{x} \in \partial B_R \mapsto w_{\text{point}}(|\mathbf{x} - \mathbf{x}_0|)$ are absolutely integrable, for some $\mathbf{x}_0 \in \partial B_R$. Moreover, assume that $\text{supp}(\phi) \subset [-\tau, \tau]$, where $\tau := \text{dist}(\text{supp}(f), \partial B_R)$ and $\text{supp}(\phi) := \{t : \phi(t) \neq 0\}$.*

Then $\mathbf{P}_{\phi,w} f \in \text{ran}(\mathbf{P})$ and

$$(\mathbf{P}^{-1} \mathbf{P}_{\phi,w} f)(\mathbf{x}) = \left[\Phi_{\text{band}} * \int_{\mathbb{R}^3} W_{\text{point}}(\cdot, \mathbf{x}') f(\mathbf{x}') d\mathbf{x}' \right] (\mathbf{x}), \quad \mathbf{x} \in B_R,$$

with the blurring kernels

$$\Phi_{\text{band}}(\mathbf{x}) := -\pi \phi'(|\mathbf{x}|)/(2|\mathbf{x}|), \quad \mathbf{x} \in \mathbb{R}^3, \quad (3)$$

$$W_{\text{point}}(\mathbf{x}, \mathbf{x}') := \frac{R^2}{|\mathbf{x}|^2} \delta(|\mathbf{x}| - |\mathbf{x}'|) w_{\text{point}}(|\mathbf{x} - \mathbf{x}'| R/|\mathbf{x}|), \quad \mathbf{x}, \mathbf{x}' \in \mathbb{R}^3. \quad (4)$$

Here δ denotes the one-dimensional delta distribution.

Proof. See Section 2. □

As a consequence of Theorem 1.1, the detector aperture causes blurring in the lateral direction, which becomes more severe near to the recording surface. The finite bandwidth, on the other hand, causes spatially invariant blurring. The two effects can be seen from Figure 2, where we numerically computed $\mathbf{P}^{-1} \mathbf{P}_{\phi,w} f$ for an initial data

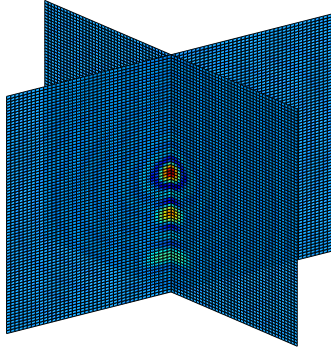


Figure 2: Resulting reconstruction by applying a numerical approximation of \mathbf{P}^{-1} to the approximate point data $\mathbf{P}_{\phi,w} f$.

f consisting of a superposition of characteristic functions of same size and a radius of the detector surface $R = 5$. For the impulse response function we have chosen the ideal low-pass filter $\phi(t) = \sin(16t)/(2t)$ and for the detector sensitivity the characteristic function $w_{\text{point}} = \chi_{[0,1/2]}$. For numerically approximating \mathbf{P}^{-1} we use a filtered back-projection type back-projection algorithm based on the third inversion formula of [11, Theorem 3].

Remark 1.2. In the case of an arbitrary domain, one obtains the same spatially invariant blurring kernel (4) due to the detector bandwidth (see Proposition 2.3). The blurring kernel (3) due to the detector size, however, depends to the shape of the detection surface. In Subsection 2.4 we also derive analytic expressions for the blurring kernel for a planar and cylindrical detection surface (Theorems 2.4, 2.5).

For detection surfaces other than spheres, planes and cylinders it seems unlikely that there exist analytic expressions for the blurring kernel due to the detector size.

1.2 Approximate line detectors

In order to partly overcome the size and shape limitations of point detectors, in [6, 34] we proposed PAT with integrating line detectors, where certain integrals of $\mathcal{W}^{3D} f$ over lines are used to reconstruct the function f . There it is assumed that

$$\Omega := \{\Phi_{\theta}(\mathbf{y}) = (y_1\theta_1, y_1\theta_2, y_2) : \theta = (\theta_1, \theta_2) \in S^1 \text{ and } \mathbf{y} = (y_1, y_2) \in D\} \quad (5)$$

is a volume of revolution generated by rotating a domain $\{0\} \times D$, with $D \subset \mathbb{R}^2$, around the $(0, 0, 1)$ axis. The data measured by ideal line detectors are given by

$$\begin{aligned} (\mathbf{L}f)(\theta, \mathbf{y}, t) &:= \int_{\mathbb{R}} (\mathcal{W}^{3D} f)(y_1\theta + s\theta^\perp, y_2, t) ds \\ &= \int_{\ell_{\theta, \mathbf{y}}} (\mathcal{W}^{3D} f)(\mathbf{z}, t) d\ell(\mathbf{z}), \quad (\theta, \mathbf{y}, t) \in S^1 \times \partial D \times (0, \infty), \end{aligned}$$

where $\ell_{\theta, \mathbf{y}} = \{\Phi_\theta(\mathbf{y}) + s(\theta^\perp, 0) : s \in \mathbb{R}^3\}$ is the unique line passing through $\Phi_\theta(\mathbf{x})$ and pointing in direction $(\theta^\perp, 0) := (-\theta_2, \theta_1, 0)$. The operator $\mathbf{L} : C_c^\infty(\Omega) \rightarrow C^\infty(S^1 \times \partial D \times (0, \infty))$ can be inverted uniquely and stably by means of a two step procedure described in [5, 13, 33]. In the case that D is a disc, exact inversion formulas are derived in [5, 10, 14, 24, 25, 29]. Efficient reconstruction methods for arbitrary domain D are again based on time reversal (see [7, 18, 19, 37]).

In practical applications line detector are usually implemented by optical line detection, where the pressure is integrated over the volume of a cylindrical laser beam. Thus, the actually available data are given by (see [32, 35])

$$(\mathbf{L}_{\phi, w} f)(\theta, \mathbf{y}, t) = \left[\phi *_t \int_{\mathbb{R}^3} w(\text{dist}(\ell_{\theta, \mathbf{y}}, \mathbf{x})) (\mathcal{W}^{3D} f)(\mathbf{x}, t) d\mathbf{x} \right] \quad \text{with } (\theta, \mathbf{y}, t) \in S^1 \times \partial D \times (0, \infty).$$

Here $w(r)$ represents the radial intensity profile of laser beam, $\ell_{\theta, \mathbf{y}}$ is its central axis, $\phi(t)$ is the impulse response function of the detection system, and $\text{dist}(\ell_{\theta, \mathbf{y}}, \mathbf{x})$ denotes the distance between the line $\ell_{\theta, \mathbf{y}}$ and the point $\mathbf{x} \in \mathbb{R}^3$. Again, application of \mathbf{L}^{-1} to the data $\mathbf{L}_{\phi, w} f$ leads to a blurred reconstruction. The laser beam, however, can be made very thin, suggesting that the one dimension approximation with approximate line detectors gives less blurred images than the zero dimension approximation with approximate point detectors.¹

Theorem 1.3. *Let $D \subset \mathbb{R}^2$, let Φ_θ, Ω be as in (5), let $f \in C_c^\infty(\Omega)$, and let $\phi, w : \mathbb{R} \rightarrow \mathbb{R}$ be even functions such that $\Phi_{\text{band}}(\mathbf{x}) = -\pi\phi'(|\mathbf{x}|)/(2|\mathbf{x}|)$ and*

$$W_{\text{line}}(\mathbf{x}) := -\frac{1}{\pi} \int_{|\mathbf{x}|}^{\infty} \frac{\partial_\xi w(\xi)}{\sqrt{\xi^2 - |\mathbf{x}|^2}} d\xi, \quad \mathbf{x} \in \mathbb{R}^3, \quad (6)$$

*are absolutely integrable. Moreover, assume that the support of $\phi * w$ satisfies $\text{supp}(\phi * w) \subset [-\tau, \tau]$, with $\tau := \text{dist}(\text{supp}(f), \partial\Omega)$.*

Then we have $\mathbf{L}_{\phi, w} f \in \text{ran}(\mathbf{L})$, and

$$(\mathbf{L}^{-1} \mathbf{L}_{\phi, w} f)(\mathbf{x}) = (\Phi_{\text{band}} * W_{\text{line}} * f)(\mathbf{x}), \quad \mathbf{x} \in \Omega.$$

¹Note that the finite length of an integrating detector does *not* influence the resolution, see [13, 35, 36].

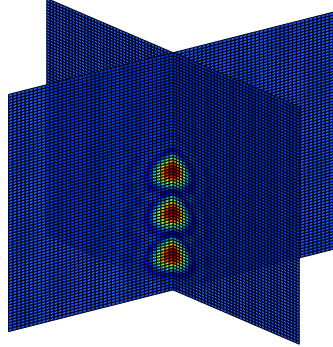


Figure 3: Result of applying a numerical approximation of \mathbf{L}^{-1} to approximate point data data $\mathbf{L}_{\phi,w} f$.

Proof. See Section 3. □

As a consequence of Theorem 1.3, the width of the laser beam and the finite bandwidth of the detection system cause spatially invariant blurring. The two effects are illustrated in Figure 3, where we numerically computed $\mathbf{L}^{-1} \mathbf{L}_{\phi,w} f$ for an initial data f consisting of a superposition of characteristic functions of same size and a spherical geometry $\Omega = B_5(0)$. For the impulse response function we have chosen the ideal low-pass filter $\phi(t) = \sin(16t)/(2t)$ and for the beam profile $w_{\text{point}}(r) = \chi_{[0,1/4]}(r) \sqrt{(1/4)^2 - r^2}$. For numerically approximating \mathbf{L}^{-1} we use a filtered back-projection type back-projection algorithm based on the second inversion formula of [10, Theorem 1.5].

1.3 Prior work and innovations

Analytic expressions for the blurring kernels with approximate line detectors are presented for the first time. Exact blurring kernels for approximate point detectors have also been derived in [41] (see [44] for an updated version) and due to the finite detector bandwidth in [4, Section 5]. However, we present a completely different and probably simpler analysis, which is based on geometric arguments and the rotational and translational invariance of the wave equation. Moreover, in [4, 41] the authors did not show that $\mathbf{P}_{\phi,w} f \in \text{ran}(\mathbf{P})$. Instead, they applied a particular inversion formula (i.e. an extension of \mathbf{P}^{-1} outside the range of \mathbf{P}) to the blurred data. Hence their results

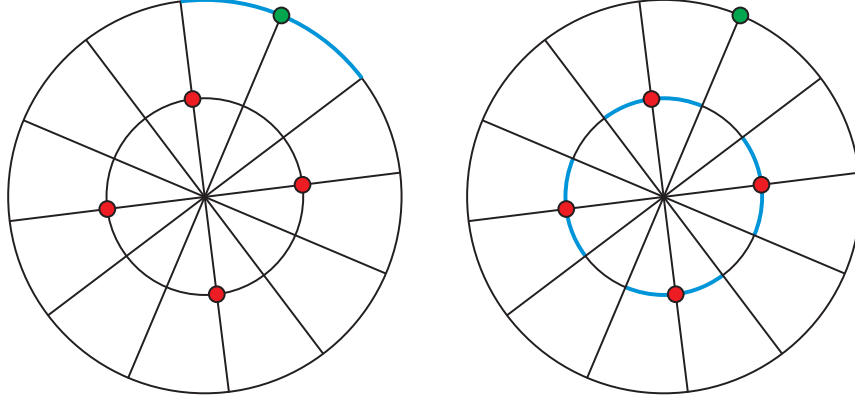


Figure 4: Left: An extended detector measures averaged signals $(\mathbf{P} f)_w$ of four point sources. Right: A point detector measures signals $\mathbf{P} f_w$ of four extended sources. Proposition 2.1 states that both signals coincide.

depend on the used extension, whereas our results are independent of any particular inversion formula.

A preliminary version of this paper has been presented at the MATHMOD 2009 conference in Vienna (see [15]) where the case $\Omega = \{x \in \mathbb{R}^3 : |x| < 1\}$ has been treated.

2 Approximate point detectors

The main goal in this section is the derivation of the analytic expressions for the blurring kernels due to the detector size and bandwidth. The proof of Theorem 1.1 will follow from Propositions 2.1 and 2.3 and will be given in Subsection 2.3.

2.1 Effects of detector size

Proposition 2.1. *Let $f \in C_c^\infty(B_R)$, let $w_{\text{point}} : \mathbb{R} \rightarrow \mathbb{R}$ be an even function such that $\mathbf{x} \in \partial B_R \mapsto w(\mathbf{x}_0, \mathbf{x}) = w_{\text{point}}(|\mathbf{x}_0 - \mathbf{x}|)$ is absolutely integrable for some $\mathbf{x}_0 \in \partial B_R$, and define, for $\mathbf{x} \in \mathbb{R}^3$,*

$$f_w(\mathbf{x}) := \int_{\mathbb{R}^3} \left[\frac{R^2}{|\mathbf{x}|^2} \delta(|\mathbf{x}| - |\mathbf{x}'|) w_{\text{point}}(|\mathbf{x} - \mathbf{x}'| R / |\mathbf{x}|) \right] f(\mathbf{x}') d\mathbf{x}'. \quad (7)$$

Then, for every $(\mathbf{x}, t) \in \partial B_R \times (0, \infty)$, we have

$$(\mathbf{P} f_w)(\mathbf{x}, t) = (\mathbf{P} f)_w(\mathbf{x}, t) := \int_{\partial B_R} w_{\text{point}}(|\mathbf{x} - \mathbf{x}'|) (\mathbf{P} f)(\mathbf{x}', t) dS(\mathbf{x}'). \quad (8)$$

Proof. We first calculate an expression for f_w without the Dirac δ distribution. To that end, denote $\mathbf{x} = \rho\sigma$, $\mathbf{x}' = \rho'\sigma'$ with $\rho, \rho' \in (0, \infty)$ and $\sigma, \sigma' \in S^2$. Then, we have

$$\begin{aligned} f_w(\mathbf{x}) &= R^2 \int_{S^2} \left(\int_0^\infty \delta(\rho - \rho') w_{\text{point}}(|\rho\sigma - \rho'\sigma'| R/\rho) f(\rho'\sigma') d\rho' \right) d\sigma' \\ &= R^2 \int_{S^2} w_{\text{point}}(|\sigma - \sigma'| R) f(\rho\sigma') d\sigma', \end{aligned}$$

which is the desired expression.

Now define, for $\mathbf{x} = \rho\sigma \in \mathbb{R}^3$ and $t \geq 0$,

$$p_w(\rho\sigma, t) := R^2 \int_{S^2} w_{\text{point}}(|\sigma - \sigma'| R) (\mathcal{W}^{3D} f)(\rho\sigma', t) d\sigma'.$$

We will show that $p_w = \mathcal{W}^{3D} f_w$, which then implies (8), since

$$p_w(R\sigma, t) = \int_{\partial B_R} w_{\text{point}}(|R\sigma - \mathbf{x}'|) (\mathcal{W}^{3D} f)(\mathbf{x}', t) dS(\mathbf{x}').$$

For every $(\vartheta, \phi) \in (0, \pi) \times (0, 2\pi)$, let $Q[\vartheta, \phi] : \mathbb{R}^3 \rightarrow \mathbb{R}^3$ denote any rotation with

$$Q[\vartheta, \phi] \mathbf{e}_3 = (\sin \vartheta \cos \phi, \sin \vartheta \sin \phi, \cos \vartheta).$$

Writing σ' in spherical coordinates around σ as north pole then shows that

$$\begin{aligned} p_w(\rho\sigma, t) &= R^2 \int_0^\pi \int_0^{2\pi} w_{\text{point}}(|\sigma - Q[\vartheta, \phi]\sigma| R) (\mathcal{W}^{3D} f)(\rho Q[\vartheta, \phi]\sigma, t) \sin \vartheta d\vartheta d\phi \\ &= R^2 \int_0^\pi w_{\text{point}}(2R(1 - \cos \vartheta)) \sin \vartheta \int_0^{2\pi} (\mathcal{W}^{3D} f)(Q[\vartheta, \phi](\rho\sigma), t) d\vartheta d\phi. \end{aligned}$$

The rotational invariance of the wave equation implies that for every $(\vartheta, \phi) \in (0, \pi) \times (0, 2\pi)$, the mapping

$$(\rho\sigma, t) \mapsto (\mathcal{W}^{3D} f)(Q[\vartheta, \phi](\rho\sigma), t)$$

is a solution of the wave equation and its linearity implies that also $p_w(\rho\sigma, t)$ is a solution of the wave equation. Since the initial conditions $p_w(\mathbf{x}, 0) = f_w(\mathbf{x})$ and $\partial_t p_w(\mathbf{x}, 0) = 0$ immediately follow from the definition of p_w this implies $p_w = \mathcal{W}^{3D} f_w$ and concludes the proof. \square

The blurring effect according to Proposition 2.1 is illustrated in Figure 4.

Remark 2.2. The main ingredient of the proof of Proposition 2.1 is the rotational invariance of the wave equation. In an analogous manner (see Subsection 2.4) one derives analytic expressions of the blurring kernel for a planar (using translational invariance) and for a cylindrical detection surface (using translational and rotational invariance).

2.2 Finite bandwidth

The following proposition deals with the blurring to the finite bandwidth of the detection system. It states that it is equivalent to either convolute the solution $\mathcal{W}^{3D} f$ in time with the function ϕ , or to convolute the initial data in space with $-\pi\phi'(|\mathbf{x}|)/(2|\mathbf{x}|)$. This fundamental and simple looking property seems to be a new result.

Proposition 2.3. *Let $f \in C_c^\infty(\mathbb{R}^3)$ and let $\phi : \mathbb{R} \rightarrow \mathbb{R}$ be an even compactly supported function such that $\Phi_{\text{band}}(\mathbf{x}) = -\pi\phi'(|\mathbf{x}|)/(2|\mathbf{x}|)$ is absolutely integrable in \mathbb{R}^3 . Then, the identity*

$$\mathcal{W}^{3D}(\Phi_{\text{band}} * f)(\mathbf{x}, t) = (\phi *_t \mathcal{W}^{3D} f)(\mathbf{x}, t)$$

holds for all $(\mathbf{x}, t) \in \mathbb{R}^3 \times (0, \infty)$ with \mathbf{x} outside the support of $\Phi_{\text{band}} * f$.

Proof. Let $\Psi(\mathbf{x}) = \psi(|\mathbf{x}|)$ be a radially symmetric absolutely integrable function of compact support. Our aim is to find an analytic expression for $\mathcal{W}^{3D}(\Psi * f)$ in terms of the solution $\mathcal{W}^{3D} f$ of (1a), (1b) and then to adjust Ψ such that $\mathcal{W}^{3D}(\Psi * f) = \phi *_t \mathcal{W}^{3D} f$ outside the support of $\Psi * f$.

The solution formula for the three dimensional wave equation (see [20]) applied to the initial data $\Psi * f$ reads

$$\mathcal{W}^{3D}(\Psi * f)(\mathbf{x}, t) = \frac{1}{4\pi} \partial_t t \int_{S^2} \left(\int_{\mathbb{R}^3} f(\mathbf{x}') \psi(|\mathbf{x} + t\omega - \mathbf{x}'|) d\mathbf{x}' \right) dS(\omega).$$

Substituting $\mathbf{x}' = \mathbf{x} + \rho\sigma$, with $\rho > 0$ and $\sigma \in S^2$, in the inner integral, and applying Fubini's Theorem leads to

$$\begin{aligned} \mathcal{W}^{3D}(\Psi * f)(\mathbf{x}, t) &= \frac{1}{4\pi} \partial_t t \int_{S^2} \left(\int_{S^2} \int_0^\infty f(\mathbf{x} + \rho\sigma) \psi(|\rho\sigma - t\omega|) \rho^2 d\rho dS(\sigma) \right) dS(\omega) \\ &= \partial_t t \int_0^\infty \int_{S^2} f(\mathbf{x} + \rho\sigma) \left(\frac{1}{4\pi} \int_{S^2} \psi(|\rho\sigma - t\omega|) dS(\omega) \right) dS(\sigma) \rho^2 d\rho \end{aligned}$$

The inner integral in the last expression is the (spherical) mean of $\Psi(\mathbf{x}) = \psi(|\mathbf{x}|)$ over a sphere with radius t centered at $\rho\sigma$. Denoting by I_ψ a primitive of $s \mapsto \psi(\sqrt{s})$, then [16, Lemma 5.1] assures that

$$\frac{1}{4\pi} \int_{S^2} \psi(|\rho\sigma - t\omega|) dS(\omega) = \frac{I_\psi((\rho+t)^2) - I_\psi((\rho-t)^2)}{4t\rho},$$

for $\rho, t > 0$. Consequently

$$\mathcal{W}^{3D}(\Psi * f)(\mathbf{x}, t) = \frac{1}{4} \partial_t \int_0^\infty \left(I_\psi((\rho+t)^2) - I_\psi((\rho-t)^2) \right) \left(\rho \int_{S^2} f(\mathbf{x} + \rho\sigma) dS(\sigma) \right) d\rho.$$

Differentiating under the integral leads

$$\mathcal{W}^{3D}(\Psi * f)(\mathbf{x}, t) = \frac{1}{2} \int_0^\infty (\rho - t) \psi(|\rho - t|) \left(\rho \int_{S^2} f(\mathbf{x} + \rho\sigma) dS(\sigma) \right) d\rho \quad (9)$$

for $\mathbf{x} \notin \text{supp}(\Psi * f)$.

On the other hand, we have

$$(\phi *_t \mathcal{W}^{3D} f)(\mathbf{x}, t) = \frac{1}{4\pi} \int_0^\infty \phi'(t - \rho) \left(\rho \int_{S^2} f(\mathbf{x} + \rho\sigma) dS(\sigma) \right) d\rho. \quad (10)$$

The right hand sides in equations (9) and (10) coincide if $s\psi(|s|) = -\frac{\pi}{2}\phi'(s)$ for all $s \in \mathbb{R} \setminus \{0\}$. Since ϕ is assumed to be an even function, this is the case if

$$\psi(s) = -\frac{\pi}{2} \frac{\phi'(s)}{s}, \quad s > 0.$$

By taking $\Psi = \Phi_{\text{line}}$, this concludes the proof. \square

Now we are ready to prove Theorem 1.1.

2.3 Proof of Theorem 1.1

Propositions 2.1 and 2.3 imply that

$$\begin{aligned} (\mathbf{P}_{\phi,w} f)(\mathbf{x}, t) &= \left(\phi *_t \int_{\partial B_R} w_{\text{point}}(|\mathbf{x} - \mathbf{x}'|) (\mathcal{W}^{3D} f)(\mathbf{z}', \cdot) dS(\mathbf{x}') \right) (t) \\ &= \left(\phi *_t (\mathcal{W}^{3D} f_w)(\mathbf{x}, \cdot) \right) (t) = \left(\mathcal{W}^{3D} (\Phi_{\text{band}} * f_w) \right) (\mathbf{x}, t) \end{aligned}$$

if $\mathbf{x} \notin \text{supp}(\Phi_{\text{band}} * f)$. Here f_w is defined as in (7). Together with support hypothesis on ϕ this shows that $\mathbf{P}_{\phi,w} f = \mathbf{P}(\Phi_{\text{band}} * f_w)$. Therefore $\mathbf{P}_{\phi,w} f \in \text{ran}(\mathbf{P})$ and $\mathbf{P}^{-1} \mathbf{P}_{\phi,w} f = \Phi_{\text{band}} * f_w$ which concludes the proof.

2.4 Planar and cylindrical detection surface

For the following theorems recall the definition of the data (2) of approximate point detectors.

Theorem 2.4 (Blurring kernels for planar detection surface). *Let $\Omega := (0, \infty) \times \mathbb{R}^2$ denote a half space in \mathbb{R}^3 and assume that $w(\mathbf{x}, \mathbf{x}') = w_{\text{point}}(\mathbf{x} - \mathbf{x}')$, where w_{point} is an absolutely integrable function defined on $\partial\Omega = \{0\} \times \mathbb{R}^2$. Moreover, let $f \in C_c^\infty(\Omega)$, let $\phi : \mathbb{R} \rightarrow \mathbb{R}$ be an even function such that $\Phi_{\text{band}}(\mathbf{x}) = -\pi\phi'(|\mathbf{x}|)/(2|\mathbf{x}|)$ is integrable, and assume that $\text{supp}(\phi) \subset [-\tau, \tau]$, where $\tau := \text{dist}(\text{supp}(f), \partial B_R)$.*

Then $\mathbf{P}_{\phi,w} f \in \text{ran}(\mathbf{P})$ and

$$(\mathbf{P}^{-1} \mathbf{P}_{\phi,w} f)(\mathbf{x}) = (\Phi_{\text{band}} * W_{\text{point}} * f)(\mathbf{x}), \quad \mathbf{x} \in \Omega,$$

with the blurring kernel

$$W_{\text{point}}(x, \mathbf{y}) := \delta(x) w_{\text{point}}(0, \mathbf{y}), \quad \text{for } \mathbf{x} = (x, \mathbf{y}) \in \Omega.$$

Proof. Theorem 2.4 is proven along the lines of Theorem 1.1. For showing an analogue of Proposition 2.1, one uses the translational invariance of the wave equation. \square

In the case of cylindrical surface the blurring kernel is a combination of the planar and the spherical case and follows from the translational and the rotational invariance of the wave equation.

Theorem 2.5 (Blurring kernels for cylindrical detection surface). *Let $\Omega := \mathbb{R} \times D_R$ denote a circular cylinder of radius R , and assume that*

$$w(\mathbf{x}, \mathbf{x}') = w_{\text{point}}(x - x', |\mathbf{y} - \mathbf{y}'|), \quad \text{for } \mathbf{x} = (x, \mathbf{y}), \mathbf{x}' = (x', \mathbf{y}') \in \partial\Omega.$$

Here $w_{\text{point}}(x, |\mathbf{y} - \mathbf{y}_0|)$ is assumed to be absolutely integrable on $\partial\Omega = \mathbb{R} \times \partial D_R$ for some $\mathbf{y}_0 \in \partial D_R$. Moreover, let $f \in C_c^\infty(\Omega)$, let $\phi : \mathbb{R} \rightarrow \mathbb{R}$ be an even function such that $\Phi_{\text{band}}(\mathbf{x}) = -\pi\phi'(|\mathbf{x}|)/(2|\mathbf{x}|)$ is integrable, and assume that $\text{supp}(\phi) \subset [-\tau, \tau]$, where $\tau := \text{dist}(\text{supp}(f), \partial\Omega)$.

Then $\mathbf{P}_{\phi, w} f \in \text{ran}(\mathbf{P})$, and

$$(\mathbf{P}^{-1} \mathbf{P}_{\phi, w} f)(\mathbf{x}) = \left[\Phi_{\text{band}} * \int_{\mathbb{R}^3} W_{\text{point}}(\cdot, \mathbf{x}') f(\mathbf{x}') d\mathbf{x}' \right](\mathbf{x}), \quad \text{for } \mathbf{x} = (x, \mathbf{y}) \in \Omega$$

where

$$W_{\text{point}}((x, \mathbf{y}), (x', \mathbf{y}')) := \frac{R}{|\mathbf{y}'|} \delta(|\mathbf{y}| - |\mathbf{y}'|) w_{\text{point}}(x - x', |\mathbf{y} - \mathbf{y}'|),$$

for $\mathbf{x} = (x, \mathbf{y})$ and $\mathbf{x}' = (x', \mathbf{y}') \in \Omega = \mathbb{R} \times D_R$.

Proof. Theorem 2.5 is again proven along the lines of Theorem 1.1. In order to show an analogue of Proposition 2.1, one uses the translational and the rotational invariance of the wave equation. \square

3 Approximate line detectors

In this section we derive the analytic expressions for the blurring kernels due to the detector size and bandwidth given in Theorem 1.3. In the following let $\mathcal{W}^{2D} : C_c^\infty(\mathbb{R}^2) \rightarrow C^\infty(\mathbb{R}^2 \times (0, \infty))$ denote the operator that maps a compactly supported initial data to the solution of the two dimensional wave equation

$$(\partial_t^2 - \Delta) p(\mathbf{x}, t) = 0, \quad (\mathbf{x}, t) \in \mathbb{R}^2 \times (0, \infty), \quad (11a)$$

$$p(\mathbf{x}, 0) = f(\mathbf{x}), \partial_t p(\mathbf{x}, 0) = 0, \quad \mathbf{x} \in \mathbb{R}^2. \quad (11b)$$

We will make use of the following simple Lemma.

Lemma 3.1 (Acoustic reciprocal principle in two dimensions). *Let $f \in C_c^\infty(\mathbb{R}^2)$ and let Ψ be a compactly supported absolutely integrable function. Then $\Psi * (\mathcal{W}^{2D} f) = \mathcal{W}^{2D}(\Psi * f)$.*

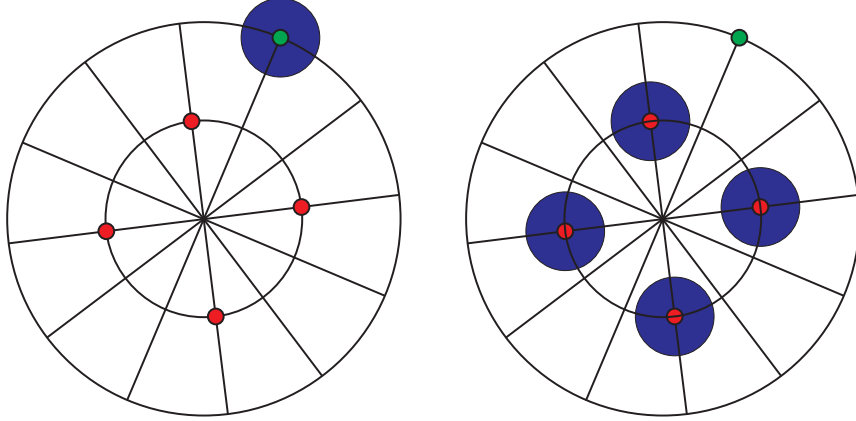


Figure 5: Left: An extended detector (with profile Ψ) measures signals of four point sources. Right: A point detector measures signals of four extended sources (with profiles Ψ). Lemma 3.1 states that both signals coincide.

Proof. D'Alembert's formula for the solution of (11a), (11b) states that $(\mathcal{W}^{2D} f)(\mathbf{x}, t) = \partial_t (g * f)(\mathbf{x}, t)$, where

$$g(\mathbf{x}, t) := \begin{cases} 1/(2\pi\sqrt{t^2 - |\mathbf{x}|^2}), & \text{if } t > |\mathbf{x}|, \\ 0, & \text{otherwise,} \end{cases}$$

see [20]. (The function $G(\mathbf{x}, \mathbf{x}', t) := g(\mathbf{x} - \mathbf{x}', t)$ is the Greens function of the two dimensional wave equation.) The symmetry of the convolution implies that

$$\Psi * (\mathcal{W}^{2D} f) = \Psi * \partial_t (g * f) = \partial_t (\Psi * g * f) = g * \partial_t (\Psi * f) = \mathcal{W}^{2D} (\Psi * f),$$

and concludes the proof. \square

Remark 3.2. Often, the term ‘‘acoustic reciprocal principle’’ simply refers to the symmetry property $G(\mathbf{x}, \mathbf{x}', t) = G(\mathbf{x}', \mathbf{x}, t)$ of the Greens function. It means that a signal induced by a point like source at position \mathbf{x}' and measured by point like detector at location \mathbf{x} remains unchanged if the source and the detector position are interchanged. It is well known that this form of the reciprocal principle also holds in the case of non-constant sound speed.

Our version of the the acoustic reciprocal principle as stated in Lemma 3.1 is more general because it also allows extended detectors represented by Ψ , see Figure 5. However, besides the symmetry, the proof of Lemma 3.1 also requires the translational invariance of the Greens function. Therefore our version of the acoustic reciprocal principle does not hold for non-constant sound speed.

3.1 Finite width of laser beam

First we calculate the blurring kernel due to the detector size.

Proposition 3.3. *Let $f \in C_c^\infty(\mathbb{R}^3)$, let $w : \mathbb{R} \rightarrow \mathbb{R}$ be a compactly supported even function such that $W_{\text{line}}(\mathbf{x}) = -1/\pi \int_{|\mathbf{x}|}^\infty \partial_\xi w(\xi) / \sqrt{\xi^2 - |\mathbf{x}|^2} d\xi$ is absolutely integrable. Then, for any line $\ell \subset \mathbb{R}^3$, we have*

$$\int_{\mathbb{R}^3} w(\text{dist}(\ell, \mathbf{x})) (\mathcal{W}^{3D} f)(\mathbf{x}, t) d\mathbf{x} = \int_\ell \mathcal{W}^{3D} (W_{\text{line}} * f)(\mathbf{x}, t) d\ell(\mathbf{x}),$$

with W_{line} as defined in (6).

Proof. Without loss of restriction we shall assume that ℓ is of the form $\ell = \mathbb{R}(1, 0, 0) + (0, y_1, y_2)$. Moreover we write $\mathbf{x} = (x, \mathbf{y})$ with $x \in \mathbb{R}$ and $\mathbf{y} = (y_1, y_2)$ in \mathbb{R}^2 , and denote by \mathbf{X} the X-ray transform restricted to lines pointing in $(1, 0, 0)$ direction,

$$(\mathbf{X} h)(\mathbf{y}) := \int_{\mathbb{R}} h(x, \mathbf{y}) dx_1, \quad h \in C_c^\infty(\mathbb{R}^3).$$

The commutation relation of the Laplacian with the X-ray transform (see [17]) implies that $\mathcal{W}^{2D} \mathbf{X} = \mathbf{X} \mathcal{W}^{3D}$. After writing $\mathbf{x}' = (x', \mathbf{y}')$ with $x' \in \mathbb{R}$ and $\mathbf{y}' = (y'_1, y'_2)$ in \mathbb{R}^2 , we obtain

$$\begin{aligned} & \int_{\mathbb{R}^3} w(\text{dist}(\ell, \mathbf{x})) (\mathcal{W}^{3D} f)(\mathbf{x}', t) d\mathbf{x}' \\ &= \int_{\mathbb{R}^2} \int_{\mathbb{R}} w(|\mathbf{y} - \mathbf{y}'|) (\mathcal{W}^{3D} f)((x', \mathbf{y}'), t) dx' d\mathbf{y}' \\ &= \int_{\mathbb{R}^2} w(|\mathbf{y} - \mathbf{y}'|) (\mathbf{X} \mathcal{W}^{3D} f)(\mathbf{y}', t) d\mathbf{y}' \\ &= (w(|\cdot|) * (\mathbf{X} \mathcal{W}^{3D} f))(\mathbf{y}, t) = (w(|\cdot|) * (\mathcal{W}^{2D} \mathbf{X} f))(\mathbf{y}, t). \end{aligned} \quad (12)$$

Now let $U(\mathbf{x}) = u(|\mathbf{x}|)$ be any radially symmetric integrable function. Then one easily verifies that $(\mathbf{X} U)(\mathbf{y}) = I_u(|\mathbf{y}|)$ with $I_u(\xi) := \int_{\mathbb{R}} u((s^2 + \xi^2)^{1/2}) ds$. Moreover, the relation $\mathbf{X} \mathcal{W}^{3D} = \mathcal{W}^{2D} \mathbf{X}$, the convolution theorem for the X-ray transform, and the acoustic reciprocal principle Lemma 3.1, imply

$$\begin{aligned} \int_\ell \mathcal{W}^{3D} (U * f)(\mathbf{x}, t) d\ell(\mathbf{x}') &= ((\mathbf{X} \mathcal{W}^{3D} (U * f))(\mathbf{y}, t) \\ &= (\mathcal{W}^{2D} \mathbf{X} (U * f))(\mathbf{y}, t) \\ &= (\mathcal{W}^{2D} (\mathbf{X} U * \mathbf{X} f))(\mathbf{y}, t) \\ &= (\mathcal{W}^{2D} (I_u(|\cdot|) * \mathbf{X} f))(\mathbf{y}, t) \\ &= (I_u(|\cdot|) * (\mathcal{W}^{2D} \mathbf{X} f))(\mathbf{y}, t). \end{aligned} \quad (13)$$

Consequently the left hand sides of (12) and (13) coincide, if

$$w(\xi) = I_u(\xi) = \int_{\mathbb{R}} u((s^2 + \xi^2)^{1/2}) ds = 2 \int_{\xi}^{\infty} u(\eta) \frac{\eta d\eta}{\sqrt{\eta^2 - \xi^2}}.$$

This is an Abel integral equation for the function u . Its solution is (see [12, 28]) $u(\eta) = -\frac{1}{\pi} \int_{\eta}^{\infty} \frac{\partial_{\xi} w(\xi)}{\sqrt{\xi^2 - \eta^2}} d\xi$. This concludes the proof by taking $W_{\text{line}} = U$. \square

3.2 Finite bandwidth

Next we calculate the point spread function due to the finite bandwidth.

Proposition 3.4. *Let $f \in C_c^{\infty}(\mathbb{R}^3)$ and let $\phi : \mathbb{R} \rightarrow \mathbb{R}$ be an even compactly supported function such that $\Phi_{\text{band}}(\mathbf{x}) = -\pi\phi'(|\mathbf{x}|)/(2|\mathbf{x}|)$ is absolutely integrable. Then*

$$\phi *_{\ell} \int_{\ell} (\mathcal{W}^{3D} f)(\mathbf{x}', t) d\ell(\mathbf{x}') = \int_{\ell} (\mathcal{W}^{3D} (\Phi_{\text{band}} * f))(\mathbf{x}', t) d\ell(\mathbf{x}') \quad (14)$$

for any line ℓ with $\ell \cap \text{supp}(\Phi_{\text{band}} * f) = \emptyset$.

Proof. Proposition 2.3 states that $\phi *_{\ell} (\mathcal{W}^{3D} f) = \mathcal{W}^{3D} (\Phi_{\text{band}} * f)$ outside the support of $\Phi_{\text{band}} * f$. Integrating this identity over ℓ proves (14). \square

3.3 Proof of Theorem 1.3

According to Propositions 3.3 and 3.4 we have

$$\begin{aligned} \phi *_{\ell} \int_{\mathbb{R}^3} w(\text{dist}(\ell, \mathbf{x}')) (\mathcal{W}^{3D} f)(\mathbf{x}, t) d\mathbf{x}' &= \phi *_{\ell} \int_{\ell} \mathcal{W}^{3D} (W_{\text{line}} * f)(\mathbf{x}', t) d\ell(\mathbf{x}') \\ &= \int_{\ell} \mathcal{W}^{3D} (\Phi_{\text{band}} * W_{\text{line}} * f)(\mathbf{x}', t) d\ell(\mathbf{x}'). \end{aligned}$$

By taking $\ell = \ell_{\theta, \mathbf{y}}$, $\mathbf{y} \in D$, and using the support hypothesis on $\phi * w$, this shows $\mathbf{L}_{\phi, w} f = \mathbf{L}(\Phi_{\text{band}} * W_{\text{line}} * f)$. Therefore $\mathbf{L}_{\phi, w} f \in \text{ran}(\mathbf{L})$ and $\mathbf{L}^{-1} \mathbf{L}_{\phi, w} f = \Phi_{\text{band}} * W_{\text{line}} * f$, which concludes the proof.

4 Discussion

In this paper we derived analytic expression for the point spread functions in PAT due to the finite detector size and the finite bandwidth of the ultrasound detection system for approximate point and approximate line detectors. We showed, that the point spread function Φ_{band} due to the finite bandwidth is spatial invariant in both cases. The point spread function due to the detector size is only spatial invariant in the case of line detectors (see Theorems 1.1 and Theorems 1.3). As the constant sound speed assumption was crucial for the presented analysis (see Proposition 2.1, Proposition 2.3, and Lemma 3.1) it seems impossible to carry over our results to the

case of arbitrary non-constant sound speed. However similar results may be obtained if the sound speed satisfies certain symmetry properties.

The intensity profile of the detecting laser beam is often well approximated by $w(r) = I_0 \exp(-\frac{r^2}{2b})$, see [32, 35]. In this case, up to some constant, the radial profile of the point spread function w_{line} coincides with the beam profile w . The full width at half maximum of the point spread function is a typical parameter to measure spatial resolution. Ignoring effects of finite bandwidth, Theorems 1.1 and 1.3 show that the lateral resolution of PAT with approximate point detectors is $a_{\text{trans}} |\mathbf{x}| / R$, where a_{trans} is the diameter of the ultrasound transducer, and the (uniform) resolution of PAT with approximate line detectors is given by the width a_{laser} of the detecting laser beam. Typical values $a_{\text{trans}} = 1 \text{ cm}$ and $a_{\text{laser}} = 0.1 \text{ cm}$ (see [32, 41]) point out the high spatial resolution of PAT with integrating line detectors.

Finally, note that in practical applications the resolution of the resulting reconstruction will also be influenced by the discrete sampling and the particular choice of the image reconstruction algorithm. Moreover, attenuation of ultrasound waves limits the bandwidth of the detected signals and therefore also limits the resolution of the final reconstruction. A quantitative analysis of the influence of those effects to the resolution of photoacoustic imaging has not been given so far.

5 Acknowledgement

This work has been supported by the Austrian Science Foundation (FWF), project S10505-N20.

References

- [1] M. L. Agranovsky and P. Kuchment. Uniqueness of reconstruction and an inversion procedure for thermoacoustic and photoacoustic tomography with variable sound speed. *Inverse Probl.*, 23(5):2089–2102, 2007.
- [2] M. L. Agranovsky and E. T. Quinto. Injectivity sets for the Radon transform over circles and complete systems of radial functions. *J. Funct. Anal.*, 139(2):383–414, 1996.
- [3] G. Ambartsoumian and P. Kuchment. On the injectivity of the circular Radon transform. *Inverse Probl.*, 21(2):473–485, 2005.
- [4] M. A. Anastasio, D. Zhang, J. Modgil, and P. L. La Riviere. Application of inverse source concepts to photoacoustic tomography. *Inverse Probl.*, 23(6):S21–S35, 2007.
- [5] P. Burgholzer, J. Bauer-Marschallinger, H. Grün, M. Haltmeier, and G. Paltauf. Temporal back-projection algorithms for photoacoustic tomography with integrating line detectors. *Inverse Problems*, 23(6):S65–S80, 2007.

- [6] P. Burgholzer, C. Hofer, G. Paltauf, M. Haltmeier, and O. Scherzer. Thermoacoustic tomography with integrating area and line detectors. *IEEE Trans. Ultrason., Ferroelectr., Freq. Control*, 52(9):1577–1583, September 2005.
- [7] P. Burgholzer, G. J. Matt, M. Haltmeier, and G. Paltauf. Exact and approximate imaging methods for photoacoustic tomography using an arbitrary detection surface. *Phys. Rev. E*, 75(4):046706, 2007.
- [8] C. Clason and M. Klibanov. The quasi-reversibility method for thermoacoustic tomography in a heterogeneous medium. *SIAM J. Sci. Comp.*, 30(1):1–23, 2007.
- [9] R. O. Esenaliev, I. V. Larina, K. V. Larin, D. J. Deyo, M. Motamedi, and D. S. Prough. Optoacoustic technique for noninvasive monitoring of blood oxygenation: a feasibility study. *App. Opt.*, 41(22):4722–4731, 2002.
- [10] D. Finch, M. Haltmeier, and Rakesh. Inversion of spherical means and the wave equation in even dimensions. *SIAM J. Appl. Math.*, 68(2):392–412, 2007.
- [11] D. Finch, S. Patch, and Rakesh. Determining a function from its mean values over a family of spheres. *SIAM J. Math. Anal.*, 35(5):1213–1240, 2004.
- [12] R. Gorenflo and S. Vessella. *Abel integral equations*, volume 1461 of *Lecture Notes in Mathematics*. Springer-Verlag, Berlin, 1991. Analysis and applications.
- [13] M. Haltmeier. Frequency domain reconstruction for photo- and thermoacoustic tomography with line detectors. *Math. Models Methods Appl. Sci.*, 19(2):283–306, 2009.
- [14] M. Haltmeier, O. Scherzer, P. Burgholzer, R. Nuster, and G. Paltauf. Thermoacoustic tomography and the circular Radon transform: exact inversion formula. *Math. Models Methods Appl. Sci.*, 17(4):635–655, 2007.
- [15] M. Haltmeier, O. Scherzer, and G. Zangerl. Influence of detector bandwidth and detector size to the resolution of photoacoustic tomography. In F. Breiteneker and I. Troch, editors, *Argesim Report no. 35: Proceedings Mathmod 09 Vienna*, pages 1736–1744, 2009.
- [16] M. Haltmeier, T. Schuster, and O. Scherzer. Filtered backprojection for thermoacoustic computed tomography in spherical geometry. *Math. Methods Appl. Sci.*, 28(16):1919–1937, 2005.
- [17] S. Helgason. *The Radon Transform*, volume 5 of *Progress in Mathematics*. Birkhäuser, Boston, second edition, 1999.
- [18] Y. Hristova. Time reversal in thermoacoustic tomography—an error estimate. *Inverse Probl.*, 25(5):055008 (14pp), 2009.
- [19] Y. Hristova, P. Kuchment, and L. Nguyen. Reconstruction and time reversal in thermoacoustic tomography in acoustically homogeneous and inhomogeneous media. *Inverse Problems*, 24(5):055006 (25pp), 2008.

- [20] F. John. *Partial Differential Equations*, volume 1 of *Applied Mathematical Sciences*. Springer Verlag, New York, fourth edition, 1982.
- [21] R. A. Kruger, W. L. Kiser, D. R. Reinecke, G. A. Kruger, and K. D. Miller. Thermoacoustic molecular imaging of small animals. *Mol. Imaging*, 2(2):113–123, 2003.
- [22] R. A. Kruger, P. Lui, Y. R. Fang, and R. C. Appledorn. Photoacoustic ultrasound (PAUS)—reconstruction tomography. *Med. Phys.*, 22(10):1605–1609, 1995.
- [23] P. Kuchment and L. A. Kunyansky. Mathematics of thermoacoustic and photoacoustic tomography. *European J. Appl. Math.*, 19:191–224, 2008.
- [24] L. A. Kunyansky. Explicit inversion formulae for the spherical mean Radon transform. *Inverse Probl.*, 23(1):373–383, 2007.
- [25] L. A. Kunyansky. A series solution and a fast algorithm for the inversion of the spherical mean radon transform. *Inverse Probl.*, 23(6):S11–S20, 2007.
- [26] A. K. Louis and E. T. Quinto. Local tomographic methods in sonar. In *Surveys on solution methods for inverse problems*, pages 147–154. Springer, Vienna, 2000.
- [27] S. Manohar, A. Kharine, J. C. G. van Hespén, W. Steenbergen, and T. G. van Leeuwen. The Twente Photoacoustic Mammoscope: system overview and performance. *Physics in Medicine and Biology*, 50(11):2543–2557, 2005.
- [28] F. Natterer. *The Mathematics of Computerized Tomography*, volume 32 of *Classics in Applied Mathematics*. SIAM, Philadelphia, 2001.
- [29] L. V. Nguyen. A family of inversion formulas for thermoacoustic tomography. *Inverse Probl. Imaging*, 3(4):649–675, 2009.
- [30] R. Nuster, M. Holotta, C. Kremser, H. Grossauer, P. Burgholzer, and G. Paltauf. Photoacoustic micro-tomography using interferometric detection. *J. Biomed. Opt.*, 15:021307, 2010.
- [31] V. P. Palamodov. Remarks on the general Funk–Radon transform and thermoacoustic tomography. *arXiv*, page math.AP/0701204, 2007.
- [32] G. Paltauf, R. Nuster, and P. Burgholzer. Characterization of integrating ultrasound detectors for photoacoustic tomography. *Journal of Applied Physics*, 105:102026, 2009.
- [33] G. Paltauf, R. Nuster, M. Haltmeier, and P. Burgholzer. Experimental evaluation of reconstruction algorithms for limited view photoacoustic tomography with line detectors. *Inverse Problems*, 23(6):S81–S94, 2007.
- [34] G. Paltauf, R. Nuster, M. Haltmeier, and P. Burgholzer. Photoacoustic tomography using a Mach-Zehnder interferometer as an acoustic line detector. *App. Opt.*, 46(16):3352–3358, 2007.

- [35] G. Paltauf, R. Nuster, K. Passler, M. Haltmeier, and P. Burgholzer. Optimizing image resolution in three-dimensional photoacoustic tomography with line detectors. In A. Oraevsky and L. V. Wang, editors. *Photons Plus Ultrasound: Imaging and Sensing 2008: The Ninth Conference on Biomedical Thermoacoustics, Photoacoustics, and Acousto-optics*, volume 6856 of *Proceedings of SPIE*, 2008.
- [36] O. Scherzer, M. Grasmair, H. Grossauer, M. Haltmeier, and F. Lenzen. *Variational methods in imaging*, volume 167 of *Applied Mathematical Sciences*. Springer, New York, 2009.
- [37] P. Stefanov and G. Uhlmann. Thermoacoustic tomography with variable sound speed. *Inverse Probl.*, 25(7):075011, 16, 2009.
- [38] L. V. Wang. Prospects of photoacoustic tomography. *Med. Phys.*, 35(12):5758–5767, 2008.
- [39] L. V. Wang. Multiscale photoacoustic microscopy and computed tomography. *Nature Phot.*, 3(9):503–509, 2009.
- [40] X. D. Wang, G. Pang, Y. J. Ku, X. Y. Xie, G. Stoica, and L. V. Wang. Noninvasive laser-induced photoacoustic tomography for structural and functional *in vivo* imaging of the brain. *Nature Biotech.*, 21(7):803–806, 2003.
- [41] M. Xu and L. V. Wang. Analytic explanation of spatial resolution related to bandwidth and detector aperture size in thermoacoustic or photoacoustic reconstruction. *Phys. Rev. E*, 67(5):0566051–05660515 (electronic), 2003.
- [42] M. Xu and L. V. Wang. Universal back-projection algorithm for photoacoustic computed tomography. *Phys. Rev. E*, 71(1):0167061–0167067 (electronic), 2005.
- [43] M. Xu and L. V. Wang. Photoacoustic imaging in biomedicine. *Rev. Sci. Instruments*, 77(4):1–22, 2006. Article ID 041101.
- [44] M. Xu and L. V. Wang. Analysis of spatial resolution in photoacoustic tomography. In L. V. Wang, editor, *Photoacoustic imaging and spectroscopy*, chapter 5, pages 47–60. CRC Press, Boca Raton, FL, 2009.
- [45] Y. Xu, L. V. Wang, G. Ambartsoumian, and P. Kuchment. Reconstructions in limited-view thermoacoustic tomography. *Med. Phys.*, 31(4):724–733, 2004.